Crack and damage propagation in polystyrene under fatigue loading

John Botsis
Department of Civil Engineering, Mechanics and Metallurgy, University of Illinois at Chicago, Chicago, IL 60680, USA
(Received 5 May 1987; revised 18 August 1987; accepted 5 September 1987)

Fatigue crack propagation experiments conducted on thin, single edge-notched polystyrene specimens demonstrate that during quasi-static propagation intense crazing surrounds and precedes the crack. The crack and its associated damage constitute a crack layer (CL). Craze accumulation within the zone ahead of the crack tip, i.e. the active zone, takes place prior to crack advance. During crack advance, the shape of the crack tip closely resembles that of the Dugdale–Barendblatt model. The shape of the active zone is found to be dependent on loading history. Fracture surface examination reveals two types of discontinuous crack growth bands: multicycle and single-cycle bands. The total energy release rate for unit CL advance, evaluated from load–displacement curves, is found to be close to the elastic energy release rate. The variation of the ratio of active zone length to band width with the energy release rate suggests that the elastic energy release rate does not uniquely characterize the strains and stresses around the crack tip. This is attributed to intensive crazing around the crack tip. The experimental results demonstrate that fracture propagates by the translation, expansion and distortion of the active zone. The critical energy release rate is found to be strongly dependent on loading history.

(Keywords: polystyrene; fatigue; damage; crack layer; active zone; translation; expansion; distortion)

INTRODUCTION

Concepts of fracture mechanics are extensively used to describe fatigue crack propagation (FCP) in different materials. Thus, several models have been proposed which attempt to relate the crack growth rates to some function of the stress intensity factor K_1, for linear elastic fracture mechanics, or the energy release rate J_1, for nonlinear fracture mechanics. They differ only with respect to the emphasis they place on the variables and concomitant assumptions. They share, however, the assumption that fracture propagation is described by one geometric parameter, i.e. the crack length. One limitation of this approach is demonstrated by considering FCP kinetics over a wide range of propagation rates. In addition, recent work[1-4] with different materials has shown that crack deceleration occurs with increasing K_1 or J_1. This type of behaviour cannot be explained by the existing FCP theories since they all predict a monotonic increase of crack speed with increasing K_1 or J_1.

In recent years a significant amount of experimental work has accumulated which demonstrates that a zone of severely damaged material, adjacent to the crack tip, precedes the propagating crack. This zone is usually termed a plastic zone[5], process zone[6,7], dissipation zone[8] or deformation zone[9]. It has been observed that for polymers the damage constituting a process zone may be in the form of crazes[10,11], shear bands[12], a combination of both[13] or homogeneous deformation[9,14]; martensitic transformation in ceramics[15]; microcracking in concrete[16] and rock[17]; and slip planes and microcracking in metals[18].

Recently, a crack layer (CL) theory[19,20] has been proposed to model fracture phenomenon as observed. The system consisting of a crack and the surrounding damage is considered as a macroscopic entity and called a CL. The zone adjacent to the crack tip, where damage accumulates prior to fracture, is identified as the active zone. CL theory models fracture propagation in terms of active zone movements. In general this zone may translate, rotate as a rigid body and deform.

The objective of this report is to examine the mechanisms of FCP using polystyrene (PS) as a model material and employing time-lapse optical microscopy simultaneously with crack propagation measurements. The experiments are aimed at determining which of the four degrees of freedom, proposed by the CL theory, controls fatigue crack growth. The results described herein consist of both macro- and microscopic studies. The macroscopic studies include analysis of the kinetics of the crack and the evolution of the surrounding damage, while microscopic studies consist of fracture surface examination.

EXPERIMENTAL PROCEDURES

Single edge-notched tension specimens of 80 mm gauge length, 20 mm width and 0.25 mm thickness of plane isotropic PS were used in the investigation. The details of specimen preparation can be found elsewhere[21]. Fatigue experiments were performed on a 20 kN capacity electrohydraulic closed-loop MTS machine in a laboratory atmosphere using a sinusoidal waveform loading at a frequency of 0.2 Hz and load ratio of 0.2. An optical microscope, equipped with a motor-driven camera, attached to the MTS, was used to register crack

0032-3861/88/030457-06$03.00

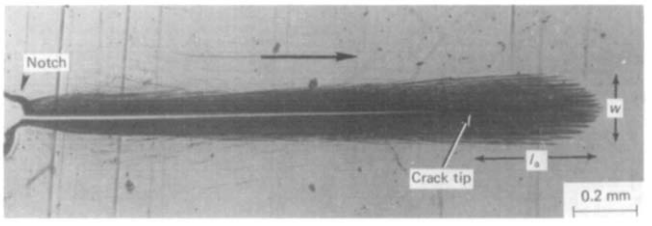

Figure 1 Optical micrograph of a CL during quasi-static propagation. Horizontal arrow indicates the direction of propagation

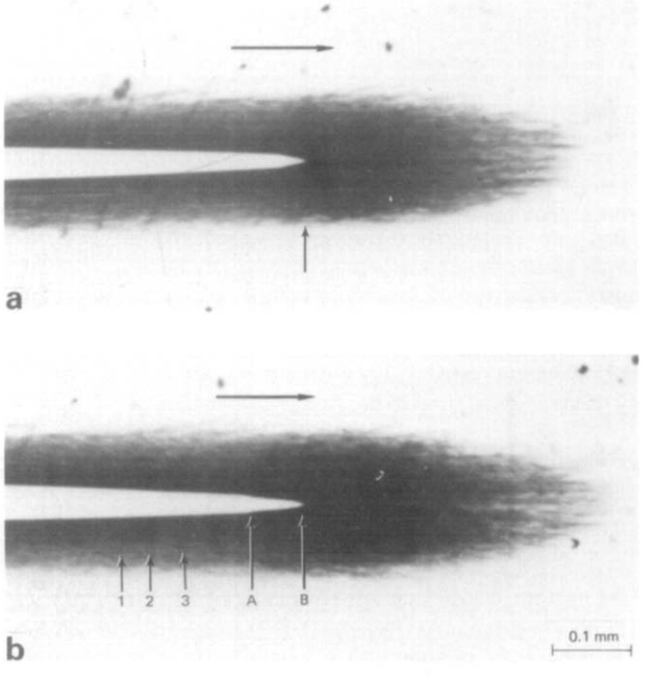

Figure 2 Real-time optical micrographs taken during the loading portion of a fatigue cycle. Note here the shape of the crack tip

advance and the surrounding damage evolution. The elastic energy release rate G_1 was calculated as K_1^2/E where E is the tensile elastic modulus of the material, which was determined experimentally ($E = 2.2$ GPa). The stress intensity factor K_1 was calculated by using the formula

$$K_1 = \sigma_{max}(\pi l)^{1/2} f(l/B)$$

where σ_{max} is the maximum applied stress of the fatigue cycle, l is the crack length, B is the specimen width and[22]

$$f(l/B) = 1.12 - 0.231(l/B) + 10.55(l/B)^2 - 21.72(l/B)^3 + 30.39(l/B)^4$$

Crack propagation data and the history of damage evolution were obtained from micrographs taken at appropriate intervals at load excursions. The micrographs were taken without interrupting the experiment. Complementary kinetic data were gained from subsequent fractographic analysis and the CL profile using optical microscopy. Thus, the measurements cover the entire range of quasi-static crack layer propagation.

RESULTS AND DISCUSSION

Crack propagation mechanisms

Previous work on FCP in PS[21,23] has shown that an intensive layer of crazing precedes and surrounds the propagating crack, thus constituting a CL. A general view of a well developed CL propagating at a mean stress $\sigma_m = 10.7$ MPa is shown in *Figure 1*. At the front of CL is an active zone. Within this zone, damage growth takes place prior to crack advance[23]. The same process is repeated until transition to dynamic (fast) fracture occurs.

Figure 2 presents two real-time optical micrographs taken during the loading portion of a fatigue cycle. The time interval between these micrographs was four cycles. During loading, the crack advances into predamaged material. The newly formed crack surfaces A–B (*Figure 2b*) do not belong on the plane of the crack. Relaxation, however, takes place within the next few fatigue cycles and the crack surfaces come down to the plane of the crack. This may be due to viscoelastic behaviour of irreversible deformation, which is associated with craze formation. Note here the relative darkness of the active zone. The dark markings (i.e. arrows 1, 2 and 3 in *Figure 2b*) perpendicular to the crack propagation direction correspond to successive portions of the crack tip. It is worth noting that the shape of the crack tip (*Figure 2*) closely resembles that of the Dugdale–Barendblatt model[24,25].

Figure 3 illustrates successive configurations of the active zone as a function of the crack length for two different loading levels. The contours are traced from optical micrographs, similar to that of *Figures 1* and *2*, taken during the experiments. Note here that the shape of the active zone is a function of the loading history. Although the width w of the active zone (*Figures 1* and *2*) is only a fraction of a millimetre on both sides of the crack, its importance in the fracture process should not be underemphasized. Specifically, the following points should be brought to attention. First, the energy expended in craze formation within the active zone is orders of magnitude higher than that expended on the crack itself[26]. Secondly, the craze layer cannot be approximated by a zone of constant width since it changes by almost an order of magnitude from initiation up to specimen failure. Thirdly, the width of the active zone at critical CL propagation is almost the same (*Figure 3*). However, the density of the respective transverse sections is significantly different. Namely,

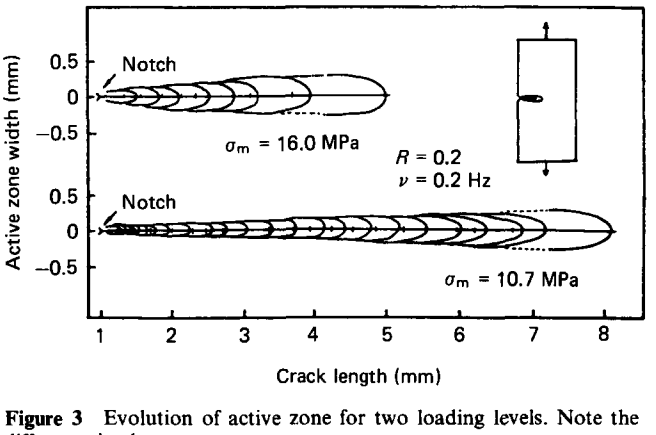

Figure 3 Evolution of active zone for two loading levels. Note the difference in shape

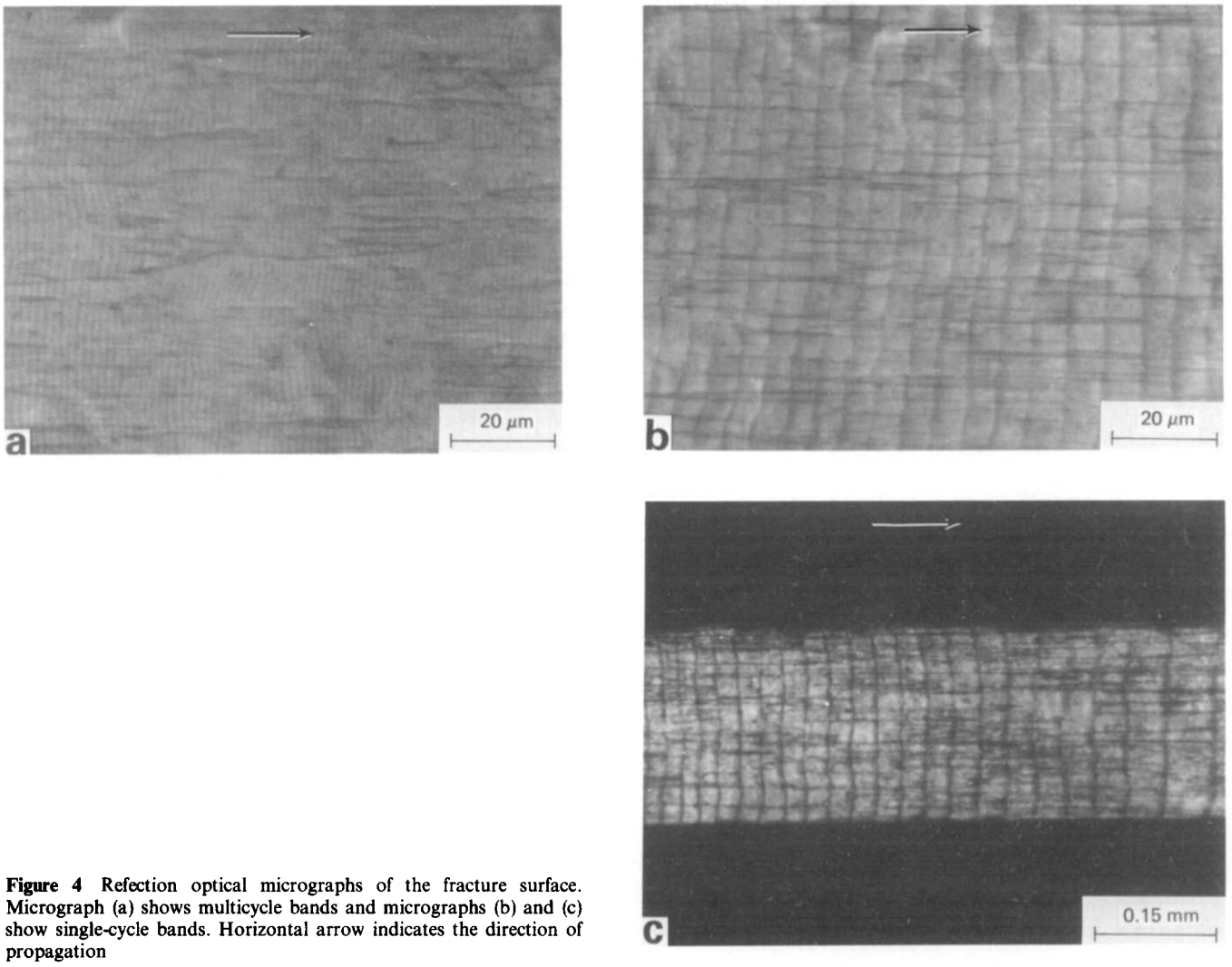

Figure 4 Refection optical micrographs of the fracture surface. Micrograph (a) shows multicycle bands and micrographs (b) and (c) show single-cycle bands. Horizontal arrow indicates the direction of propagation

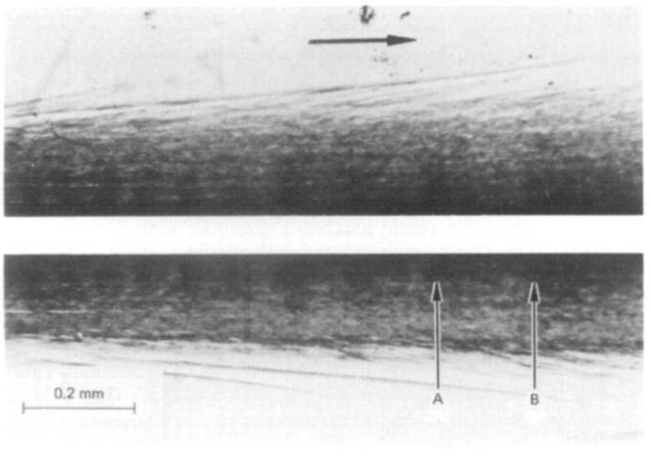

Figure 5 Optical micrograph at the single-cycle band region of two halves of a specimen after fracture. Arrows indicate positions of the crack tip

crazing density is twice as high for the lower loading level experiment[23]. These experimental observations strongly suggest that one kinematic parameter (crack length) is not enough to describe adequately the kinematics of fracture propagation. On the other hand, the theory of a CL treats the active zone as an evolving entity with several degrees of freedom[19,20].

Fractographic analysis

The nature of crack growth and fracture mechanisms may be obtained by examining the fracture surface. The optical micrographs shown in *Figure 4* exhibit discontinuous crack growth patterns, as is documented by the striated morphology of the fracture surface. The span between two strictions is usually defined as a band. The size of the band varies with the energy release rate. At relatively low levels of energy release rate (i.e. small crack length), multicycle bands are observed (*Figure 4a*). At relatively high levels of the energy release rate, one-cycle bands are observed (*Figures 4b* and *4c*). *Figure 5* shows an optical micrograph of a portion of the side view of two halves of a specimen after fracture. The dark markings (arrows, *Figures 2* and *5*) perpendicular to the fracture surface correspond to the position of the crack tip. The distance between them is equal to the band width measured from the fracture surface. The higher crazing density at these points is probably due to the highly localized irreversible deformation at the crack tip.

The striated morphology of the fracture surface has been used to extract crack growth kinetic data when both multicycle and one-cycle band growth is observed[23]. This is achieved by plotting the change in number of bands per unit crack length increment and the change in number of cycles per unit crack length increment as a function of the crack length. The point where the two curves merge marks the beginning of the single-cycle band

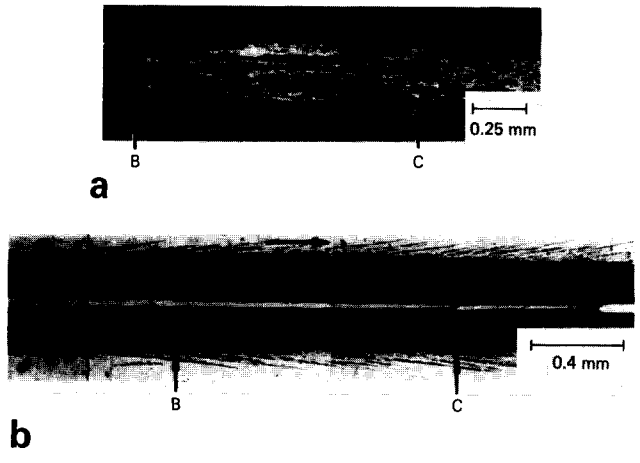

Figure 6 Fracture surface and corresponding side view at specimen fracture. Arrow B indicates the last striation and arrow C the critical crack length

region. Thus, the fracture surface provides the speed of a crack when it grows too fast to be measured by simple techniques. When the two curves coincide for the entire range of quasi-static crack propagation, then the single-cycle band mode prevails[27]. When they do not intersect, all the bands are multicycle bands. This was the case for poly(vinyl chloride) where only multicycle bands were observed throughout the entire quasi-static crack propagation[28].

Analysis of the experimental results has demonstrated that the change of active zone width decreases with the energy release rate and approaches zero near the transition to dynamic fracture[21,23]. These observations together with the change in morphology of the fracture surface are utilized to define the critical crack length from which the critical energy release rate can be calculated. *Figure 6* exhibits the portion of the fracture surface at critical CL configuration (*Figure 6a*) and the corresponding side view (*Figure 6b*). Note here the constancy of the CL width. Striation B corresponds to the last completed band during quasi-static CL propagation. The attempt of the material to form the next band is terminated by the transition to dynamic propagation.

Kinetics of fracture propagation

According to the phenomenological theory of a CL, the active zone may experience translation and rotation as a rigid body, isotropic expansion and distortion[19]. Accordingly, for rectilinear CL propagation, the total energy release rate for unit CL advance is[29]:

$$A_1 = J_1 + M\partial_l e + N_{mn}\partial_l V^d_{mn}$$

Here J_1, M and M_{mn} are the energy release rates for translation, expansion and distortion of the active zone, respectively, e is a measure of expansion, V^d_{mn} is the deviatoric part of the deformation tensor of the active zone and ∂_l denotes the partial derivative with respect to crack length. The above decomposition for the total energy release rate suggests that the area between two load–displacement curves consists of three contributions: translational, expansional and distortional.

It is worth noting that elastoplastic solutions predict plastic zones with shapes and sizes that differ in essential ways from the observed ones (*Figure 2*). Therefore, elastoplastic solutions cannot be used for energy calculations in this case. A new approach to semiempirical energy calculations based on recent developments of stress analysis of a CL[30,31] and experimental measurements is under way.

The full curve in *Figure 7* represents the elastic energy release rate calculated as $G_1 = K_1^2/E$ and the data points are measurements of the total energy release rate A_1 calculated from load–displacement curves. The data in *Figure 7* show that A_1 appears to be close to the elastic energy release rate. This is understandable in view of the small size of the active zone with respect to the crack length (i.e. $w/l \sim l_a/l \ll 1$). For polycarbonate, however, the active zone is comparatively large with respect to crack length[32]. Therefore, A_1 can only be measured from conventional techniques based on the evolution of load-displacement curves[32,33].

Figures 8a and *8b* demonstrate the evolution of the ratio $l_a/2b$ ($2b$ is the band width measured from the fracture surface) and the aspect ratio w/l_a of the active zone (*Figure 1*), respectively, as a function of the energy release rate for two fatigue experiments. Evidently, the data suggest that the energy release rate does not uniquely characterize the stresses and strains in the vicinity of the crack tip. This is due to the drastic change in the stress and strain fields caused by the intense craze zone in the neighbourhood of the crack tip (*Figure 9*). However, in view of the unavailability of a more appropriate parameter, the elastic energy release, which is found to be close to the total energy release rate A_1, will be used to correlate the kinetics of the CL.

Fracture propgation kinetics are observed under two loading conditions. Whereas the frequency and load ratio are the same, σ_m is 16.0 MPa for the first experiment and 10.7 MPa for the second. While there is no rotation of the active zone due to symmetry of the specimen and applied load, the change in the ratio w/l_a (*Figure 8b*) indicates that fracture propagation occurs by translation, expansion and distortion of the active zone.

The rate of active zone translation, which coincides with the crack growth rate, as a function of the energy release rate for both experiments is shown in *Figure 10*. At low crack velocity, the propagation data are obtained from optical micrographs taken during the experiment (*Figure 2*). Subsequently, the method described above based on fractographic analysis is used. While the rate of FCP is higher for the higher stress level experiment, the critical energy release rate for the lower stress level is

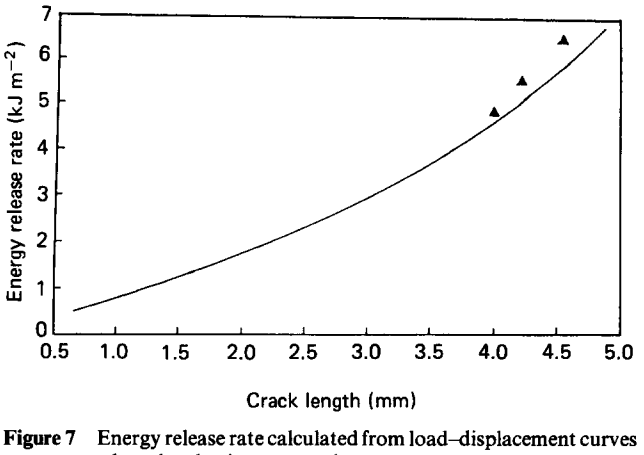

Figure 7 Energy release rate calculated from load–displacement curves as compared to the elastic energy release rate

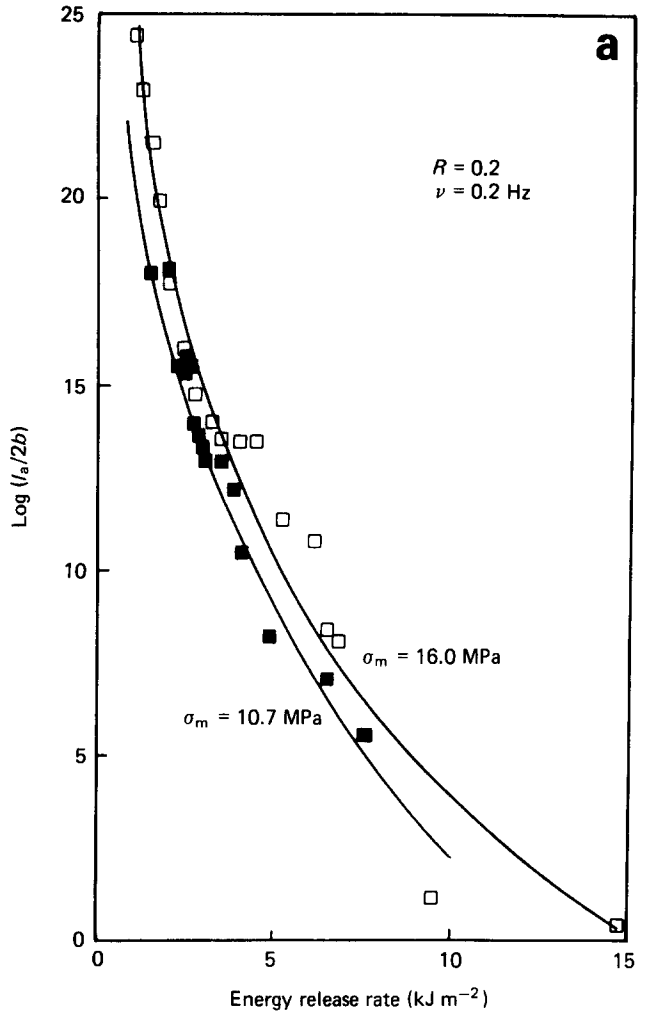

Figure 8 (a) Variation of $l_a/2b$ with the energy release rate for two levels of σ_m. (b) Variation of w/l_a with the energy release rate for two levels of σ_m

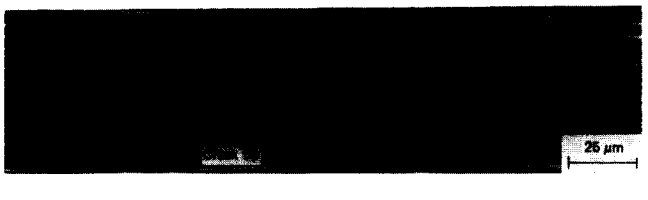

Figure 9 Optical micrograph of a polished specimen showing intensive crazing around the crack tip

almost twice that observed at the higher stress. Damage analysis of the cross-sections at critical CL propagation demonstrates that the craze intensity is significantly higher for the lower stress level experiment[21,23].

Under the assumption of homogeneous deformation within the active zone, the rate of expansion, with the crack tip as the origin:

$$\frac{de}{dN}=\frac{1}{2}\left(\frac{dw/dN}{w}+\frac{dl_a/dN}{l_a}\right)$$

and the rate of distortion:

$$\frac{dd}{dN}=\frac{1}{2}\left|\frac{dw/dN}{w}-\frac{dl_a/dN}{l_a}\right|$$

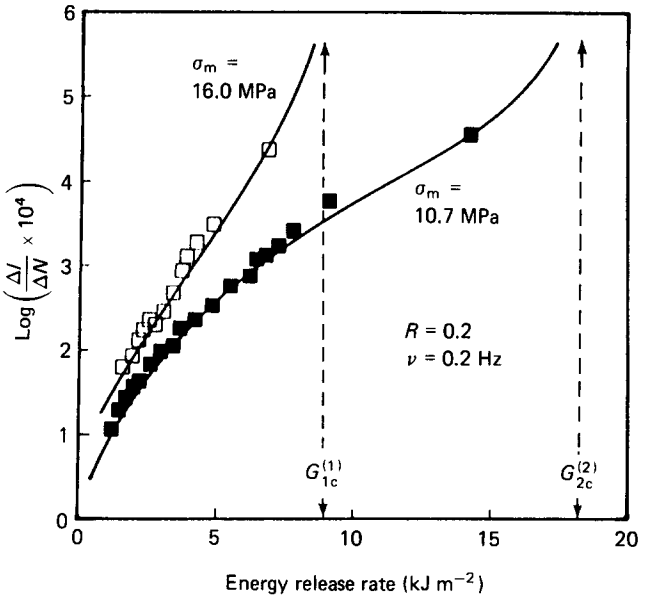

Figure 10 Crack growth kinetics plotted against the energy release rate for two levels of σ_m. Note the dependence of the critical energy release rate on σ_m

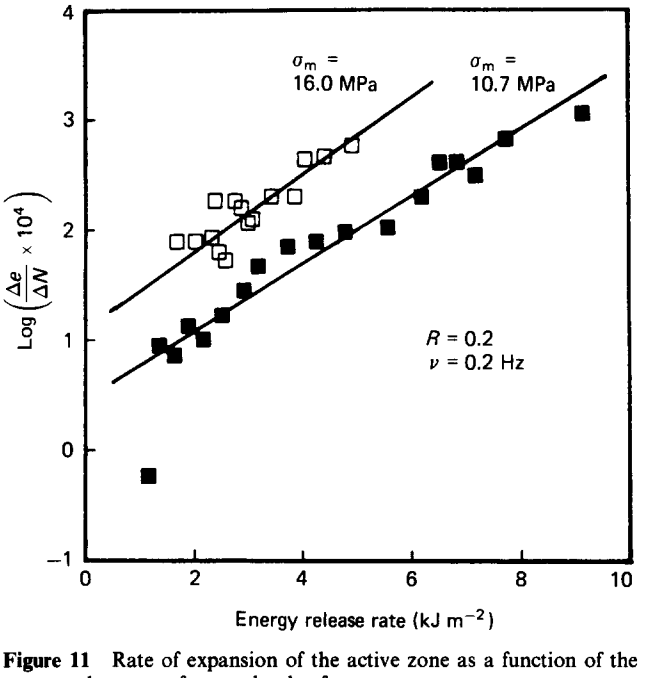

Figure 11 Rate of expansion of the active zone as a function of the energy release rate for two levels of σ_m

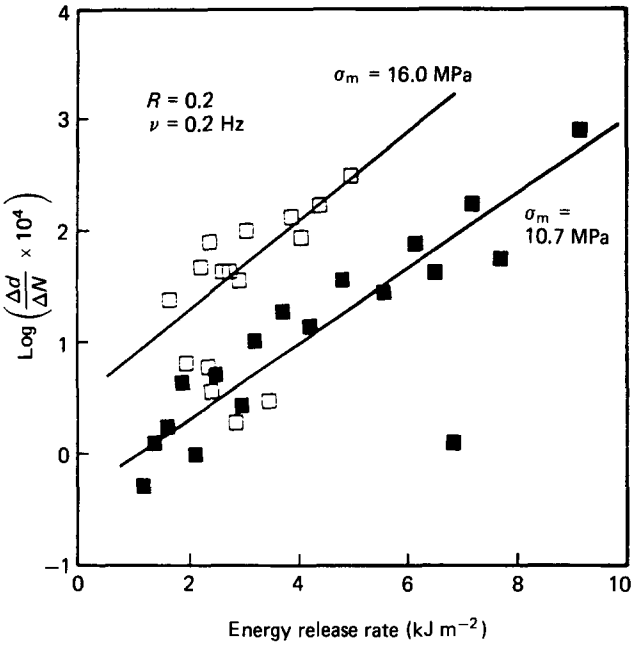

Figure 12 Rate of distortion of the active zone as a function of the energy release rate for two levels of σ_m

are obtained by decomposing the strain rate tensor into the isotropic and deviatoric parts[19]. The variations of de/dN and dd/dN with the energy release rate are shown in *Figures 11* and *12*, respectively. Note that the measurements cover the entire range of slow CL propagation.

CONCLUSIONS

Fatigue fracture in polystyrene propagates by the translation, expansion and distortion of the active zone.

The shape of the active zone and the critical energy release rate are strongly dependent on loading history.

The drastic change in stress field caused by the active zone calls for a more adequate stress analysis of the problem.

ACKNOWLEDGEMENTS

The author wishes to acknowledge the partial financial support of NASA–Lewis Center under Grant NA G3-754 and Dr K. Sehanobish for providing the data of *Figure 7*.

REFERENCES

1 Andrews, H. E. and Walker, B. J. *Proc. R. Soc.* 1971, **A325**, 57
2 Bretz, P. E., Hertzberg, R. W. and Manson, J. A. *Polymer* 1981, **22**, 1272
3 Chudnovsky, A., Moet, A., Bankert, R. J. and Takemori, M. T. *J. Appl. Phys.* 1983, **54**, 5562
4 Sandt, A. and Hornbogen, E. *J. Mater. Sci.* 1981, **19**, 2915
5 Rice, J. R. in 'Fracture', Vol. II, (Ed. H. Liebowitz), Academic Press, New York, 1964, pp. 192–308
6 Burech, F. E. in 'Fracture 1977', Vol. 3, Pergamon Press, London, 1972, p. 929
7 Claussen, N. *J. Am. Ceram. Soc.* 1976, **59**, 49
8 Pompe, H. A., Bahr, H. A., Gille, G. and Kreher, W. *J. Mater. Sci.* 1978, **13**, 2720
9 Donald, A. M. and Kramer, E. J. *J. Mater. Sci.* 1981, **16**, 2977
10 Botsis, J., Chudnovsky, A. and Moet, A. in XXIX ANTEC-SPE, Chicago, 1983, p. 444
11 Chudnovsky, A., Moet, A., Bankert, R. J. and Takemori, M. T. *J. Appl. Phys.* 1983, **54**, 5567
12 Takemori, M. T. and Kambour, R. P. *J. Mater. Sci.* 1981, **16**, 1110
13 Mills, N. J. and Walker, N. *J. Mater. Sci.* 1980, **15**, 1840
14 Andrews, A. H. and Barnes, S. P. in Int. Conf. on Deformation, Yield and Fracture of Polymers, Plastics and Rubber Institute, Cambridge, 1982, 8.1
15 Evans, G. A. and Heuer, A. H. *J. Am. Ceram. Soc.* 1980, **63**, 248
16 Carpinteri, J. *J. Struct. Div., ASCE* 1982, **ST4**, 833
17 Haglan, G. R., Hahn, A. T. and Rosenfield, A. R. *Rock Mech.* 1973, **5**, 106
18 Chudnovsky, A. and Bessendorf, M. 'Crack Layer Morphology and Toughness Characterization in Steels', NASA Contractor Report 168154, 1983
19 Chudnovsky, A., 'Crack Layer Theory', NASA Contractor Report 174634, 1984
20 Chudnovsky, A. and Moet, A. *J. Mater. Sci.* 1985, **20**, 630
21 Botsis, J. Ph.D. Dissertation, Case Western Reserve University, Cleveland, 1984
22 Tada, H., Paris, P. C. and Irwin, G. P. 'The Stress Analysis of Cracks Handbook', Del. Research Corp., Helertown, PA, 1975
23 Botsis, J., Chudnovsky, A. and Moet, A. *Int. J. Fract.* 1987, **33**, 263
24 Dugdale, D. S. *J. Mech. Phys. Solids* 1960, **8**, 100
25 Barendblatt, G. I. *Appl. Mech.* 1962, **67**, 55
26 Haddaoui, N., Chudnovsky, A. and Moet, A. *ACS Org. Coat. Appl. Polym. Chem. Proc.* 1983, **49**, 117
27 Jacoby, G. M. in 'Electron Microscopy', ASTM-STP No. 453, 1969, p. 147
28 Elink, P. J., Baumers, J. C. and Howes, G. *Int. J. Fract. Mech.* 1971, **7**, 277
29 Chudnovsky, A. *J. Appl. Mech.* to appear
30 Chudnovsky, A., Dolgopolsky, A. and Kachanov, M. *Int. J. Solids Struct.* 1987, **23**, 1
31 Chudnovsky, A., Dolgopolsky, A. and Kachanov, M. *Int. J. Solids Struct.* 1987, **23**, 11
32 Haddaoui, N., Chudnovsky, A. and Moet, A. *Polymer* 1986, **87**, 1377
33 Knott, F. J. in 'Fundamentals of Fracture Mechanics', Butterworths, London, 1979